Modeling Frequency Dynamics in Unit Commitment with a High Share of Renewable Energy

Ziyang Zhang, *Student Member, IEEE*, Ershun Du, *Member, IEEE*, Fei Teng, *Member, IEEE*, Ning Zhang, *Member, IEEE*, Chongqing Kang, *Fellow, IEEE*

***Abstract*—The power system inertia is gradually decreasing with the growing share of variable renewable energy (VRE). This may jeopardize the frequency dynamics and challenges the secure operation of power systems. In this paper, the concept of frequency security margin is proposed to quantify the system frequency regulation ability under contingency. It is defined as the maximum power imbalance that the system can tolerate while keeping frequency within the tolerable frequency range. A frequency constrained unit commitment (FCUC) model considering frequency security margin is proposed. Firstly, the analytical formulation of system frequency nadir is derived while considering both the frequency regulation characteristics of the thermal generators and the frequency support from VRE plants. Then, the frequency security margin is analytically formulated and piecewise linearized. A novel FCUC model is proposed by incorporating linear frequency security constraints into the traditional unit commitment model. Case studies on a modified IEEE RTS-79 system and HRP-38 system are provided to verify the effectiveness of the proposed FCUC model. The impacts of VRE penetration on system frequency security are analyzed using frequency security margin.**

***Index Terms*—frequency dynamics, power system inertia, unit commitment, high share of renewable energy, virtual synchronous machine.**

NOMENCLATURE

A. Indices and Sets

t	Index of the time from 1 to N_T
g	Index of the thermal generator from 1 to N_G
w	Index of the wind farm from 1 to N_W
pv	Index of the PV station from 1 to N_{PV}
l	Index of the transmission line from 1 to N_L
n	Index of the bus node from 1 to N_N
j	Index of the piecewise linear constraint from 1 to N_J
Ω_n^G	Set of the thermal generators connected at bus n
Ω_n^W	Set of the wind farms connected at bus n
Ω_n^{PV}	Set of the PV stations connected at bus n
Ω_n^{LS}	Set of transmission lines starting from bus n
Ω_n^{LE}	Set of transmission lines ending at bus n

B. Parameters

$C^{G,SU}$ / $C^{G,SD}$	Start-up/ -down cost of the thermal generator
C^G / $C_g^{G,B}$	Variable operating cost/ no-load cost of the thermal generator
$P^{G,Max}$ / $P^{G,Min}$	Maximum/minimum power output of the thermal generator
$\alpha^{G,UP}$ / $\alpha^{G,DN}$	Hourly ramp up/down capacity of the thermal generator
$T^{G,on}$ / $T^{G,off}$	Minimum on/off time of the thermal generator
$P^{W,Fore}$ / $P^{PV,Fore}$ / D^{Fore}	Forecasted power output of the wind farm/PV station/load demand
$VoLL$	Penalty cost of load curtailment
r_{load}, r_{RE}	Forecast error of the load and VRE
$F^{L,Max}$ / B^L	Capacity/susceptance of the transmission line
H^G	Inertia constant of the thermal generator
F_H^G	Fraction of power generated by the high-pressure turbine
R^G	Governor regulation constant of the thermal generator
K_m	Mechanical power gain factor.
H^W / H^{PV}	Synthetic inertia constant of the wind farm/PV station
R^W / R^{PV}	Droop coefficient of the wind farm/PV station
β^C / β^H / β^F / β^R	Coefficients of the piecewise linear constraints

This work was supported in part by the National Key R&D Program of China (No. 2016YFB0900100), the National Natural Science Foundation of China (No. 51907100), the Postdoctoral Innovative Talents Support Program (No. BX20180154), International (Regional) Joint Research Project of National Natural Science Foundation of China (No. 71961137004) and Tsinghua University Initiative Scientific Research Program (20193080026).

Corresponding author: Ning Zhang (ningzhang@tsinghua.edu.cn) and Chongqing Kang (cqkang@tsinghua.edu.cn).

Z. Zhang, E. Du, N. Zhang, and C. Kang are with the State Key Lab of Power Systems, Dept. of Electrical Engineering, Tsinghua University, Beijing, China and International Joint Laboratory on Low Carbon Clean Energy Innovation.

F. Teng is with Department of Electrical and Electronic Engineering, Imperial College London, London, UK.

$\underline{f}_{\min}$	System frequency security threshold
ΔP	Frequency security margin requirement

C. Variables

C^{sys}	System operating cost
P^G / P^W / P^{PV}	Power output of the thermal generator/wind farm/PV station
x^G	Binary variable representing the on/off status of the thermal generator
$x^{G,SU}$ / $x^{G,SD}$	Binary variable indicating the start-up/shut-down of the thermal generator
u^G / u^W / u^{PV}	Binary variable indicating whether the thermal generator/wind farm/PV station participates in the primary frequency response
D^{Cur}	Load curtailment
F^L	Power flow of the transmission line
θ	Voltage angle of the bus node
H / F / R	System equivalent inertia constant/turbine parameter/governor regulation constant
$\overline{\Delta P}$	Frequency security margin

I. Introduction

A. Motivation

The penetration of variable renewable energy (VRE) is gradually increasing all over the world. Since wind turbines and PV panels are connected to the power grid by power electronic interfaces, the power system synchronous inertia is gradually decreasing along with the growing share of VRE [1]. Such a trend would deteriorate the frequency response performance of the power system [2]. The impact of wind power penetration on system frequency dynamics is analyzed in [3]. The inherent intermittent and non-dispatchable features of wind power not only inject additional fluctuations to the already variable nature of frequency deviation but also decrease system frequency stability by reducing the inertia and the regulation capability [4], [5]. Although the interconnection of power systems can improve the system inertia and the frequency regulation capability, the system frequency dynamics may get worse, as tripping of tie-lines may lead to a larger power imbalance than the tripping of large generators [6].

In order to satisfy the inertia requirements in the power system with a high share of VRE, it is supposed to consider frequency dynamics in power system scheduling models. Traditional power system scheduling models only consider the steady-state operational constraints and ignore system frequency dynamics as there are usually enough online synchronous generators to maintain the system frequency under normal operation and contingencies [7]. In the case of the high share of VRE, the online capacity of the synchronous generators decreases, and the system has a lower level of inertia. The system frequency will drop much faster after a generation-load imbalance under contingency, which may lead to frequency security violations or even system-wide instability. More synchronous generators could be scheduled to provide inertia to ensure the system frequency security if frequency dynamics are considered in power system scheduling models.

In this paper, we explore how to model frequency dynamics in generation scheduling for power systems with a high share of VRE. A novel unit commitment (UC) model considering frequency security constraints is proposed.

B. Literature Review

Currently, there has been some literature focusing on how to incorporate frequency response constraints in power system operation models, such as optimal power flow (OPF) and UC. Restrepo *et al.* were one of the first researchers to consider frequency regulation constraints in the UC model in order to ensure the adequacy of primary and tertiary frequency reserves [8]. However, this study only considered the quasi-steady frequency rather than the frequency dynamics in which the frequency nadir happens. Chang *et al.* proposed a UC model considering the frequency nadir limit in frequency dynamics. However, the frequency nadir after contingency is estimated based on historical data, making it difficult to be generalized [9]. Chavez *et al.* developed an OPF model considering frequency security constraints according to simplified frequency dynamics, ignoring the load damping effect [10]. Inspired by this work, Wen *et al.* studied the benefits of fast-response battery energy storage in maintaining frequency dynamics security [11]. Ahmadi *et al.* proposed a system frequency response (SFR) model to analytically calculate the system frequency nadir after contingency and derive the frequency security constraints using a piecewise linearization technique [12], [13]. With the assumption that the frequency regulation reserve is delivered linearly in the frequency dynamic process, Teng *et al.* formulated linear frequency security constraints and applied them in a stochastic UC model [14]. Paturet *et al.* proposed a stochastic UC model considering the minimum inertial requirement for low-inertia systems [15]. Sokoler *et al.* proposed an optimal reserve planning model for an isolated power system to guarantee that the system frequency maintains above a pre-defined limit during the contingency [16].

With the presence of increasing VRE share in power systems, some studies have explored the techniques and benefits of providing frequency support by VRE. Xin *et al.* proposed a control strategy for PV stations to provide frequency response [17]. Yang *et al.* studied how a wind turbine can provide frequency support by releasing the kinetic energy of the revolving mass [18]. Since the control of power electronic interface is flexible, some researchers have proposed novel inverter control strategies to imitate the frequency characteristics of a mechanical rotary interface. In this way, renewable power plants can also provide inertia and primary frequency response like conventional thermal generators. This technique is commonly named virtual synchronous machine (VSM) [19]-[23]. Gevorgian *et al.* evaluated the contribution of synthetic inertia and primary frequency response from wind generation to improve the system frequency response performance [24]. Teng *et al.* evaluated the benefits of frequency support from wind farms in a generation scheduling problem [25]. Chu *et al.* proposed a stochastic system scheduling model to optimize the synthetic inertia provision from wind turbines [26].

In summary, some studies explore how to incorporate frequency security constraints in power system operation models to ensure frequency stability under contingency. Most of them consider the quasi-steady frequency and impose frequency reserve constraints to ensure the adequacy of frequency regulation reserve. Some studies consider the frequency dynamics and impose frequency security constraints to limit the frequency nadir under contingency. In this paper, instead of limiting the frequency nadir, a novel index, frequency security margin, is proposed as the maximum tolerable power imbalance under frequency security and incorporated into the UC model. The impact of VRE penetration on the frequency security margin is analyzed.

C. Contributions

Considering the literature review, the contributions of this paper are three-fold:

- The concept of frequency security margin, which denotes the maximum tolerable power imbalance in contingency, is proposed to formulate the frequency security constraints. Compared with existing researches, the proposed concept has a clear physical meaning, and the proposed frequency security constraints are linear regarding the power system scheduling decision variables. The numerical results demonstrate that the proposed linear frequency security margin constraints have high accuracy (error less than 5% with 95 piecewise linear segments).
- A frequency constrained unit commitment (FCUC) model is proposed based on frequency security margin constraints. Compared with the existing UC model considering frequency nadir limit, the proposed method is more flexible in modeling frequency security constraints. The disturbance can either be a pre-defined imbalance power or the capacity of the largest online generators/tie-line. Besides, the possible frequency support from VRE is also considered.
- Case studies on the IEEE RTS-79 system and HRP-38 system are performed to demonstrate the effectiveness of the proposed FCUC method. The results indicate that 1) the frequency constraints become binding under high VRE penetration scenarios, and 2) the proposed FCUC model can guarantee frequency security under different shares of VRE. The benefits of allowing VRE plants to provide frequency support are also quantified.

D. Paper Organization

The rest of this paper is organized as follows: Section II formulates the analytical model of frequency dynamics considering the frequency support from VRE. Section III introduces the frequency security margin. Section IV proposes the frequency constrained UC model. In Section V and Section VI, case studies based on the IEEE RTS-79 system and HRP-38 system are performed. Section VII draws conclusions.

II. Analytical Model of Frequency Dynamics Considering Frequency Support From VRE

A. Frequency Dynamics

Power system frequency is closely linked with the real-time balance of active power. Fig. 1 shows typical frequency dynamics after a generator outage. The frequency dynamics can be divided into four steps chronologically, namely, inertia frequency response, primary frequency response, secondary frequency response, and tertiary frequency response.

The inertia response takes effect immediately after the occurrence of the contingency. During this initial period, generator governors do not respond yet because of the frequency dead band. The rate of change of frequency (RoCoF) is fully determined by the system inertia. The system frequency may drop rapidly in a low-inertia system (E.g., a renewable-dominated power system). When the frequency exceeds the dead band, the governors start to adjust the output of the prime mover, and the frequency is gradually pulled back to a quasi-steady state. The frequency nadir usually occurs in this primary frequency response process. It should be noted that the value of the quasi-steady frequency has deviations from that of the nominal frequency. To further recover the system frequency to the nominal value, automatic generation control (AGC) will then be activated to adjust the output of dispatchable generators. This process is named the secondary frequency response. The tertiary frequency response refers to online economic dispatch, which aims to reschedule the generation output to recover the frequency reserve and prepare for the next possible contingency.

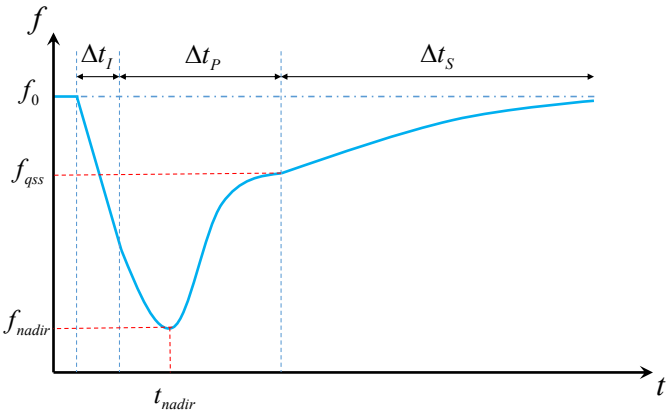

Fig. 1. Power system frequency dynamics after contingency.

The frequency dynamics can be formulated by the first-order swing equation as follows [27]:

$$2H\frac{d\Delta f(t)}{dt}+D\Delta f(t)=\Delta P_m(t)-\Delta P_e(t) \tag{1}$$

where H and D are the system inertia constant and load-damping constant, $\Delta f(t)$, $\Delta P_m(t)$ and $\Delta P_e(t)$ are the deviation of frequency, electrical power generation and power imbalance, respectively. It should be noted that if we normalize both sides of the equation using the value of total load demand, D would be a constant irrespective of the load level, and H would be solely determined by the characteristics of the thermal generator and would not be affected by its installed capacity. In the derivation of this paper, we assume that all the frequency-related equations are normalized by load demand.

During the primary frequency response, generator governors respond to the power imbalance. This process can be described using a multi-machine system frequency response (MM-SFR) model, as shown in Fig. 2.

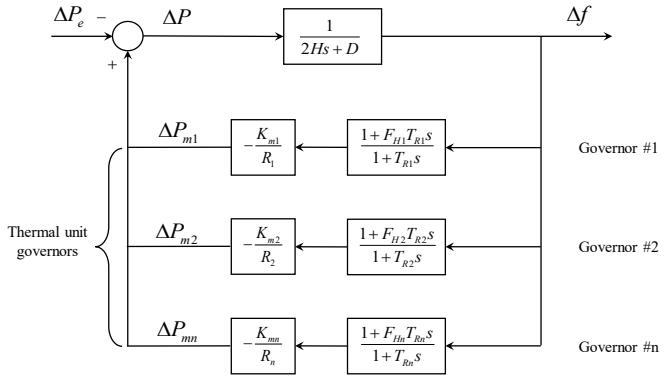

Fig. 2. Multi-machine system frequency response (MM-SFR) model.

B. Frequency Support from VRE

VRE plants are usually connected into the power system by power electronic devices, and hence they do not inherently provide inertia to the power system. Recently, a new control strategy, grid-forming inverter or VSM, is proposed to utilize the flexibility of power electronics to provide frequency support. Considering the synthetic inertia provided by VRE, the system frequency dynamics can be expressed as follows [28]:

$$2\left(H+\sum_j H_{Vj}\right)\frac{d\Delta f(t)}{dt}+D\Delta f(t)=\Delta P_m(t)+\sum_j \Delta P_{aj}(t)-\Delta P_e(t) \quad (2)$$

where H_V is the synthetic inertia and $\Delta P_a(t)$ is the output power adjustment of the VRE.

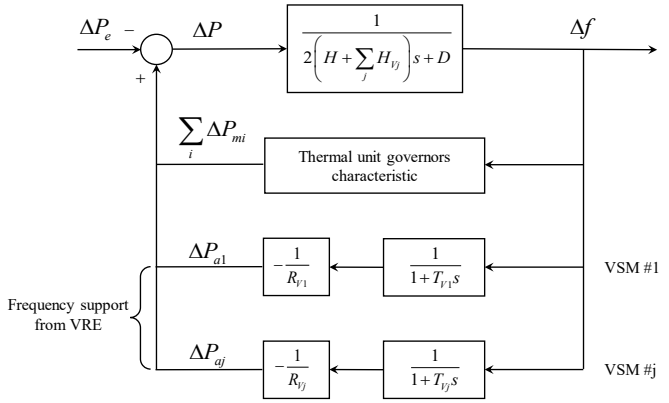

Fig. 3. System frequency model considering frequency support from VRE.

Generally, VRE plants are operated in the degeneration mode or with installed storage devices to provide the frequency regulation service. The control method mostly adopts droop control, which can be expressed by the following inertial element.

$$\Delta P_a=-\frac{1}{R_V}\frac{1}{1+sT_V}\Delta f \quad (3)$$

where R_V is the droop coefficient and T_V is a time constant representing the response speed of the inverter.

The detailed MM-SFR model considering frequency support from VRE is shown in Fig. 3.

C. Estimating the Frequency Nadir

Although it is difficult to obtain an analytical expression of the frequency with the MM-SFR model, an equivalent aggregated system frequency (ASFR) model is proposed in [29] with an acceptable approximation error, as shown in Fig. 4. The detailed derivation from the MM-SFR model to the ASFR model can be found in [29].

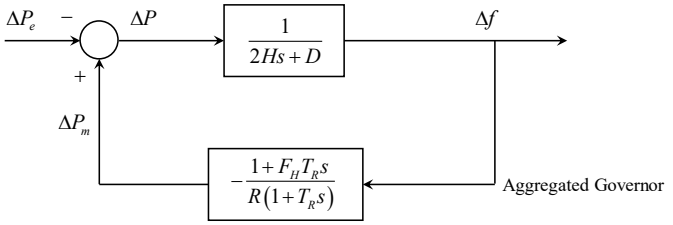

Fig. 4. Aggregated system frequency model.

According to the ASFR model, an analytical expression of the frequency dynamics after a step disturbance ΔP can be derived.

$$\Delta f(t)=\frac{R\Delta P}{DR+1}\left[1+\alpha e^{-\zeta\omega_n t}\sin(\omega_r t+\varphi)\right] \quad (4)$$

where

$$\begin{cases} \omega_n{}^2=\dfrac{DR+1}{2HRT_R} \\ \zeta=\dfrac{DRT_R+2HR+F_H T_R}{2(DR+1)}\omega_n \\ \omega_r=\omega_n\sqrt{1-\zeta^2} \\ \alpha=\sqrt{\dfrac{1-2T_R\zeta\omega_n+T_R^2\omega_R^2}{1-\zeta^2}} \\ \phi=\arctan\left(\dfrac{\omega_r T_R}{1-\zeta\omega_n T_R}\right)-\arctan\left(\dfrac{\sqrt{1-\zeta^2}}{-\zeta}\right) \end{cases} \quad (5)$$

T_R is the reheat time constant. The physical meanings of ω_n, ζ, ω_r, α, and ϕ can be found in [29].

According to (4), the frequency nadir can be derived as (6). Since we normalize the above equations with the load demand, the value of load damping constant D remains constant. Equation (6) shows that the frequency nadir f_{nadir} is determined by parameters H, R, F_H, which are the outputs of the generation scheduling, and the level of power imbalance ΔP.

$$\begin{cases} t_{nadir}=\dfrac{1}{\omega_r}\tan^{-1}\left(\dfrac{\omega_r T_R}{\zeta\omega_r T_R-1}\right) \\ \Delta f_{nadir}=\dfrac{R\Delta P}{DR+1}\left(1+\sqrt{1-\zeta^2}\alpha e^{-\zeta\omega_n t_{nadir}}\right) \\ f_{nadir}=f_0-\Delta f_{nadir} \end{cases} \quad (6)$$

III. Frequency Security Margin

This section proposes a novel concept referred as frequency security margin. It transforms the frequency nadir constraints into the capacity reserve constraints which are easier to be understood and linearized in UC.

A. Frequency Security Margin

The frequency security is usually built as an inequality in which the frequency nadir is supposed to be larger than a pre-defined threshold determined by system operators.

$$f_{nadir} \geq \underline{f}_{\min} \tag{7}$$

According to (6), the frequency deviation threshold corresponds to a maximum power disturbance. We name this power as the frequency security margin. It can be estimated by

$$\overline{\Delta P}=\left(f_0-\underline{f}_{\min}\right) g\left(H,F_H,R\right) \tag{8}$$

where

$$g\left(H,F_H,R\right)=\frac{DR+1}{R\left(1+\sqrt{1-\zeta^2}\alpha e^{-\zeta\omega_n t_{nadir}}\right)} \tag{9}$$

According to the definition of frequency security margin, it is the upper bound of power imbalance that leads to the frequency nadir within the pre-defined threshold. Therefore, limiting the frequency nadir is equivalent to limiting the power disturbance below the frequency security margin:

$$\overline{\Delta P} \geq \Delta P \tag{10}$$

where ΔP is determined by the largest disturbance, e.g., the maximum thermal generator output or the tie-line capacity.

According to (9), the formulation of $g\left(H,F_H,R\right)$ is nonlinear with respect to parameters H,F_H,R, which is illustrated in Fig. 5. Thus, it is difficult to directly incorporate (10) into the UC model.

B. Linearizing the Frequency Security Margin

In this subsection, we linearize the function $g\left(H,F_H,R\right)$ using the following piecewise linearization method.

First, a series of sample points $\left(H_k,F_{Hk},R_k,g_k\right)$ is derived from (9), where $g_k=g\left(H_k,F_{Hk},R_k\right)$. We choose the parameter space as $\left(H_k,\frac{F_{Hk}}{R_k},\frac{1}{R_k}\right)\in S$ and divide S into a series of subspaces $S_j\left(j=1,2,\quad,N_J\right)$. The reason we choose the parameter space as $\left(H_k,\frac{F_{Hk}}{R_k},\frac{1}{R_k}\right)$ is that the three parameters can be linearly expressed by the decision variables in the UC model, which is further explained in the next section. In each subspace $S_j\left(j=1,2,\quad,N_J\right)$, the following optimization model is used to find the closest hyperplane to $g\left(H,F_H,R\right)$:

$$\begin{aligned}&\min \sum_{k\in S_j} Err_k\\ &s.t.\quad \forall k\in S_j\\ &\begin{cases}Err_k=g\left(H_k,F_{Hk},R_k\right)-\left(\beta_j^C+\beta_j^H H_k+\beta_j^F\frac{F_{Hk}}{R_k}+\beta_j^R\frac{1}{R_k}\right)\\ Err_k\geq 0\end{cases}\end{aligned} \tag{11}$$

where $\beta_j^C,\beta_j^H,\beta_j^F,\beta_j^R\left(j=1,2,\quad,N_J\right)$ are the coefficients that determine the hyperplanes.

Then, the frequency security margin $\overline{\Delta P}$ can be estimated by the minimum value of the linear approximation $\overline{\Delta P_j}$ among all subspaces $S_j\left(j=1,2,\quad,N_J\right)$:

$$\overline{\Delta P_j}=\left(f_0-\underline{f}_{\min}\right)\cdot\left(\beta_j^C+\beta_j^H H+\beta_j^F\frac{F_H}{R}+\beta_j^{\frac{1}{R}}\frac{1}{R}\right) \tag{12}$$

The linearization error can be controlled by the number of subspaces. The lower figure in Fig. 5 shows the relative error of the approximation. The maximum error is limited to under 5% when the number of subspaces $N_J=95$.

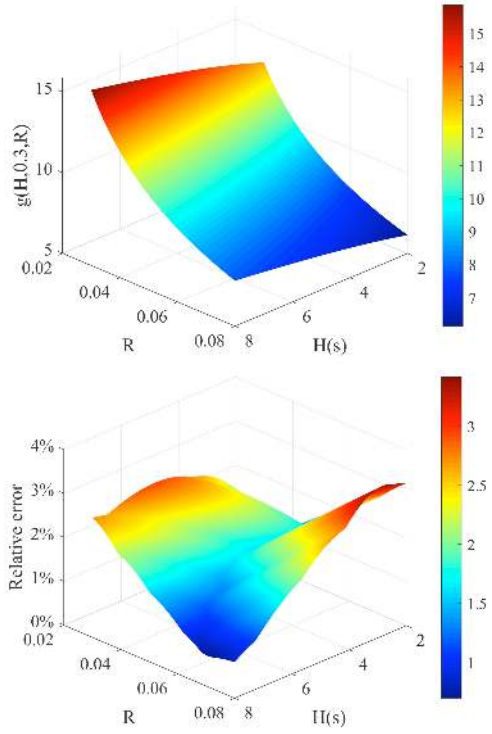

Fig. 5. The upper figure shows the function $g(H,F_H,R)$ for F_H=0.3. The lower figure shows the relative error of the approximation.

Then, equation (10) can be transformed into a series of linear frequency security margin constraints shown in (13). It should be noted that the fitting results are conservative because the piecewise linear constraints (13) are stricter than (10).

$$\left(f_0-\underline{f}_{\min}\right)\left(\beta_j^C+\beta_j^H H+\beta_j^F\frac{F_H}{R}+\beta_j^{\frac{1}{R}}\frac{1}{R}\right)\geq\Delta P,\quad\forall j \tag{13}$$

C. Discussion

Though the proposed model may look similar to the work of Paturet [15], the two papers have several significant differences. This paper proposes a novel concept referred as frequency security margin. It transforms the frequency nadir constraints into the capacity reserve constraints which are easier to be understood and linearized in UC. The frequency security margin requirement ΔP in equation (13) could either be a fixed parameter or a decision variable in the UC model, such as the

thermal generators' output or transmission power of tie-line. In addition, this paper adopts the linear programming (LP) to achieve the piecewise linearization. As shown in formulation (11), the approximation error is required to be non-negative. This guarantees that the linearized frequency constraint (13) is stricter than the original constraint (10). Besides, the inter-dependency between system inertia and governor characteristics is also captured using the hyperplanes to approximate the frequency security margin.

IV. UC Model Considering Frequency Dynamics

This section integrates the frequency security margin constraints (13) into a UC model. We firstly introduce the traditional UC model and then describe how to link the variables of traditional UC with the frequency constraints.

A. Traditional Unit Commitment (TUC)

The objective function is to minimize the operating cost, including the start-up cost, shut-down cost and variable operating cost of the thermal generators and the load shedding cost, over time periods from 1 to N_T. Though the cost model is linear, it can be extended to nonlinear cost curves using a constrained cost variable technique originally utilized in MATPOWER.

Minimize

$$C^{sys}=\sum_{t=1}^{N_T}\sum_{g=1}^{N_G}\left(C_g^{G,SU}x_{g,t}^{G,SU}+C_g^{G,SD}x_{g,t}^{G,SD}+C_g^{G}P_{g,t}^{G}+C_g^{G,B}x_{g,t}^{G}\right)+\sum_{t=1}^{N_T}\sum_{n=1}^{N_N}VoLL\ D_{n,t}^{Cur} \quad (14)$$

1) Node active power balance constraints

$$\sum_{g\in\Omega_n^G}P_{g,t}^{G}+\sum_{w\in\Omega_n^W}P_{w,t}^{W}+\sum_{pv\in\Omega_n^{PV}}P_{pv,t}^{PV}-\sum_{l\in\Omega_n^{LS}}F_{l,t}^{L}+\sum_{l\in\Omega_n^{LE}}F_{l,t}^{L}=D_{n,t}^{Fore}-D_{n,t}^{Cur}\quad\forall n,\forall t \quad (15)$$

$$0\le D_{n,t}^{Cur}\le D_{n,t}^{Fore}\quad\forall n,\forall t \quad (16)$$

Equation (15) ensures a balance between the load demand and generation at each node for each period. Equation (16) limits the load shedding to less than the load demand.

2) Transmission capacity constraints

$$F_{l,t}^{L}=B_l^{L}\left(\theta_{l(+),t}-\theta_{l(-),t}\right),\forall l,\forall t \quad (17)$$

$$-\pi\le\theta_{n,t}\le\pi\ ,\forall l,\forall t \quad (18)$$

$$-F_l^{L,Max}\le F_{l,t}^{L}\le F_l^{L,Max}\ ,\forall l,\forall t \quad (19)$$

Equation (17) represents the DC power flow model of each transmission line. Equation (18) limits the phase angle of each node. Equation (19) limits the power flow of each branch to its capacity.

3) Operational constraints of the thermal generators

$$x_{g,t}^{G}P_g^{G,Min}\le P_{g,t}^{G}\le x_{g,t}^{G}P_g^{G,Max}\ ,\forall g,\forall t \quad (20)$$

$$x_{g,t}^{G,SU}-x_{g,t}^{G,SD}=x_{g,t}^{G}-x_{g,t-1}^{G}\ ,\forall g,\forall t \quad (21)$$

$$x_{g,t}^{G},x_{g,t}^{G,SU},x_{g,t}^{G,SD}\in\{0,1\}\ ,\forall g,\forall t \quad (22)$$

$$P_{g,t}^{G}-P_{g,t-1}^{G}\le x_{g,t-1}^{G}\alpha_{g,t}^{G,UP}+x_{g,t}^{G,SU}P_g^{G,Min}\ ,\forall g,\forall t \quad (23)$$

$$P_{g,t-1}^{G}-P_{g,t}^{G}\le x_{g,t-1}^{G}\alpha_{g,t}^{G,DN}+x_{g,t}^{G,SD}P_g^{G,Min}\ ,\forall g,\forall t \quad (24)$$

$$\sum_{\tau=t-T_g^{G,on}-1}^{t-1}x_{g,\tau}^{G}\ge x_{g,t}^{G,SD}T_g^{G,on}\ ,\forall g,\forall t \quad (25)$$

$$\sum_{\tau=t-T_g^{G,off}-1}^{t-1}\left(1-x_{g,\tau}^{G}\right)\ge x_{g,t}^{G,SU}T_g^{G,off}\ ,\forall g,\forall t \quad (26)$$

Equation (20) limits the output of the thermal generator to $\left[P_g^{G,Min},P_g^{G,Max}\right]$ when online and to zero when offline. Equations (21) and (22) show the relationships among the on/off status variable, start-up variable and shut-down variable. Equations (23) and (24) are the ramp limits. Equations (25) and (26) limit the minimum online and offline time.

4) Renewable energy operational constraints

$$0\le P_{w,t}^{W}\le P_{w,t}^{W,Fore}\ ,\forall w,\forall t \quad (27)$$

$$0\le P_{pv,t}^{PV}\le P_{pv,t}^{PV,Fore}\ ,\forall pv,\forall t \quad (28)$$

Equations (27) and (28) limit the output power of the VRE plants to not larger than the forecasted production.

5) System reserve constraints

$$\sum_g x_{g,t}^{G}P_g^{G,Max}+\sum_w P_{w,t}^{W,Fore}+\sum_{pv}P_{pv,t}^{PV,Fore}+\sum_b P_b^{B,Max}+\sum_n D_{n,t}^{Cur}\ge\left(1+r_{Load}\right)\sum_n D_{n,t}^{Fore}+r_{RE}\left(\sum_w P_{w,t}^{W,Fore}+\sum_{pv}P_{pv,t}^{PV,Fore}\right)\quad\forall t \quad (29)$$

Equation (29) ensures that the online capacity of generation can satisfy the load demand considering the forecast errors of VRE and the load.

B. Frequency Security Margin Constraints

As described in section II.C, the frequency security margin can be estimated by a series of linear constraints using parameters $H,\frac{F_H}{R},\frac{1}{R}$. To integrate the constraints into the UC model, the parameters $H,\frac{F_H}{R},\frac{1}{R}$ are expressed by the operation status of generation units and are shown in (30)~(32).

$$H_t=\frac{1}{\sum_n D_{n,t}^{Fore}}\left(\begin{array}{l}\sum_g x_{g,t}^{G}H_g^{G}P_g^{G,Max}+\sum_w u_{w,t}^{W}H_w^{W}P_{w,t}^{W,Fore}\\+\sum_{pv}u_{pv,t}^{PV}H_{pv}^{PV}P_{pv,t}^{PV,Fore}\end{array}\right),\forall t \quad (30)$$

$$F_t=\frac{1}{\sum_n D_{n,t}^{Fore}}\left(\sum_g u_{g,t}^{G}\frac{K_{mg}F_g^{G}}{R_g^{G}}P_g^{G,Max}\right),\forall t \quad (31)$$

$$\frac{1}{R_t}=\frac{1}{\sum_n D_{n,t}^{Fore}}\left(\begin{array}{l}\sum_g u_{g,t}^{G}\frac{K_{mg}}{R_g^{G}}P_g^{G,Max}+\sum_w u_{w,t}^{W}\frac{1}{R_w^{W}}P_{w,t}^{W,Fore}\\+\sum_{pv}u_{pv,t}^{PV}\frac{1}{R_{pv}^{PV}}P_{pv,t}^{PV,Fore}\end{array}\right),\forall t \quad (32)$$

Equations (30)~(32) are formulated as linear constraints of the status variables $x_{g,t}^{G}$ of the thermal generator and frequency

regulation decision variables $u_{g,t}^{G}, u_{w,t}^{W}, u_{pv,t}^{PV}$. The derivation of the three constraints is given in the Appendix. By substituting (30)~(32) into (13), the linear frequency security margin constraints are formed for each time period. It should be noted that the proposed formulating method is flexible in modeling the frequency security margin constraints. A disturbance ΔP can either be a pre-defined fixed value or the capacity of the largest online generators, which is determined by $x_{g,t}^{G}$.

Equations (33)~(35) indicate that a certain amount of output spaces of responsive units should be reserved to provide primary frequency response.

$$P_{g}^{G,Max} - P_{g,t}^{G} \geq u_{g,t}^{G} \frac{K_{mg}}{R_{g}^{G}} P_{g}^{G,Max} \kappa \left(f_0 - \underline{f}_{\min} \right), \forall g, \forall t \quad (33)$$

$$P_{w}^{W,Fore} - P_{w,t}^{W} \geq u_{w,t}^{W} \frac{1}{R_{w}^{W}} P_{w}^{W,Fore} \kappa \left(f_0 - \underline{f}_{\min} \right), \forall w, \forall t \quad (34)$$

$$P_{pv}^{PV,Fore} - P_{pv,t}^{PV} \geq u_{pv,t}^{PV} \frac{1}{R_{pv}^{PV}} P_{pv}^{PV,Fore} \kappa \left(f_0 - \underline{f}_{\min} \right), \forall pv, \forall t \quad (35)$$

It should be noted that the frequency nadir $\left(f_0 - \underline{f}_{\min} \right)$ is generally larger than the quasi-steady frequency. Thus, the reasonable value of parameter κ is less than 1.0. According to the numerical analysis, κ can be set to 0.5 in this paper.

Equation (36) indicates that only online thermal generators can provide the primary frequency response.

$$0 \leq u_{g,t}^{G} \leq x_{g,t}^{G}, u_{g,t}^{G} \in \{0,1\}, \forall g, \forall t \quad (36)$$

In summary, the formulations from (14) to (36) compose the proposed FCUC model which is a MILP problem and can be efficiently solved by off-the-shelf solvers.

V. Case Study I: IEEE RTS-79 System

A. Data Source

A case study on a modified IEEE RTS-79 system is provided to verify the effectiveness of the proposed method. The modified generation mix is shown in TABLE I. The transmission line and load demand information can be found in reference [30]. The parameters of thermal generators are listed in TABLE II. The performance of two models, namely, the TUC and proposed FCUC models, is compared. ΔP is set to 200 MW. Both models are implemented in GAMS and solved by CPLEX on a PC with 16GB of RAM and an Intel Core i7/1.8 GHz processor. The optimality gap is set to 0.1%

TABLE I
Modified generation mix of IEEE RTS-79 system (unit: MW)

Node	U155	U350	U76	U197	Wind	PV	Sum
B1	-	-	76*2	-	500	-	652
B3	-	-	76*2	-	-	500	652
B7	155*2	-	-	-	-	-	310
B13	-	-	-	197*3	-	-	591
B15	-	-	76*2	-	-	-	252
B16	-	-	76*2	-	500	-	652
B18	-	350*2	-	-	-	-	700
B21	-	350	-	-	500	-	850
B22	-	350	-	-	-	500	850
B23	155*2		-	-	-	500	810
Total	620	1400	608	591	1500	1500	6319

TABLE II
Parameters of the thermal generators

Generation type	U155	U350	U76	U197
Capacity (MW)	155	350	76	197
Variable cost ($/MWh)	30	20	45	35
No-load cost($/h)	0	0	0	0
Start-up cost ($/MW)	2	4	6	6
Shut-down cost ($/MW)	2	4	6	6
Minimum online time (h)	8	8	4	4
Minimum offline time (h)	8	8	4	4
Ramp capacity	50%	50%	80%	80%
Minimum output	35%	50%	20%	20%
Inertia constant (s)	6	8	4	6
Governor constant	0.05	0.05	0.033	0.033

TABLE III shows the frequency response characteristic of the thermal generators and VRE plants. The ability of VRE for frequency support is set based on [31]. Since the ability of the grid forming inverter installed in VRE has a large range, we make a conservative assumption that frequency support ability is 50% of those of conventional thermal generators per capacity.

TABLE III
Frequency response characteristics of the thermal generators and VRE plants

Generation type	U155	U350	U76	U197	Wind	PV
Inertia constant (s)	6	8	4	6	3	2
Turbine factor F_H	0.3	0.35	0.25	0.3	-	-
Governor constant	0.05	0.05	0.033	0.033	-	-
Droop of VRE	-	-	-	-	0.067	0.067

The output curves of wind power and PV are obtained from SAM software developed by NREL. The following figure shows the forecasted power of renewables used in the case study. To highlight frequency security issues, we select forecasted wind power with the anti-peak regulation feature.

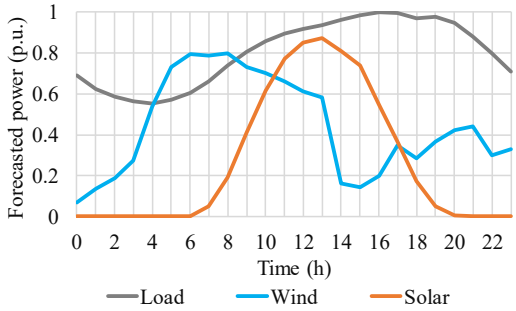

Fig. 6. Forecasted load demand and VRE outputs.

B. Results

We set the system nominal frequency to 50 Hz and the minimum frequency threshold to 49.5 Hz. The results of the TUC and FCUC models are summarized in TABLE IV. Imposing frequency constraints leads to a 2.31% increase in operating cost and more renewables curtailment. The generation schedule is shown in Fig. 7. Compared with the TUC model, imposing frequency constraints leads to more

synchronous units scheduled online from time period 4h to 17h to guarantee frequency security.

We use the MM-SFR model to test the frequency security of both results. Fig. 8 compares the frequency dynamics for both models when encountering a 200 MW power imbalance at time period 14h. The results indicate that the frequency nadir of TUC is lower than 49.5 Hz, while in FCUC, it is maintained above the threshold 49.5 Hz.

TABLE IV
Comparison of the results of TUC and FCUC

	Operating cost ($)	Wind curtailment	PV curtailment
FCUC	713997	3.62%	4.80%
TUC	697864	1.61%	3.00%

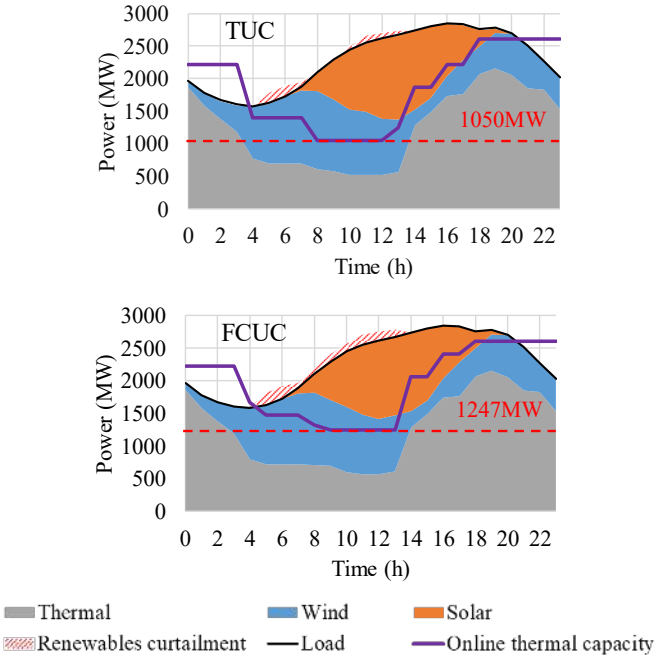

Fig. 7. Power generation results of TUC (upper) and FCUC (lower).

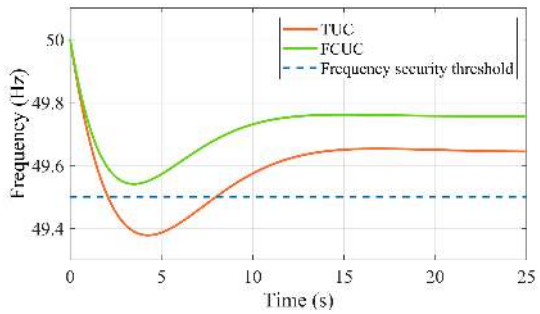

Fig. 8. Frequency dynamics after contingency of FCUC and TUC.

The frequency security margin reflects the system's capability to withstand a contingency. Fig. 9 compares the frequency security margin of TUC and FCUC. FCUC ensures that the system can tolerate the power imbalance no more than 200 MW during the whole time. For the TUC results, the frequency security margin is below the required value for most of the time. Especially from time period 6h to 18h, several thermal generators are shut down when a large amount of VRE is available, which leads to low system inertia and thus a low frequency security margin. The results indicate the effectiveness and necessity to incorporate frequency constraints into the generation scheduling model.

Fig. 10 analyses the relationship between frequency security margin and the share of VRE in power generation. The frequency security margin of the operating points of TUC and FCUC are compared using a scatter diagram under different instantaneous VRE share from 5% to 80%. We set the frequency security margin requirements as 200MW for all time. The findings of the case study are: 1) The frequency security margins of TUC are strongly driven by the VRE penetration. In this case, when VRE penetration is lower than 32%, the set frequency security margin requirements are inherently satisfied. When VRE penetration is higher than 32%, the system would face the risk of frequency insecurity. 2) The proposed FCUC model enables more synchronous inertia and frequency regulating resources to meet the frequency security requirement by optimizing the operation of thermal generators and renewable generation. The results imply that: 1) High VRE penetration would decrease the system inertia and weaken the system frequency regulation ability. 2) The proposed frequency security margin is a useful index to reflect the system frequency security under contingency. 3) The proposed FCUC model can guarantee frequency security under different shares of VRE.

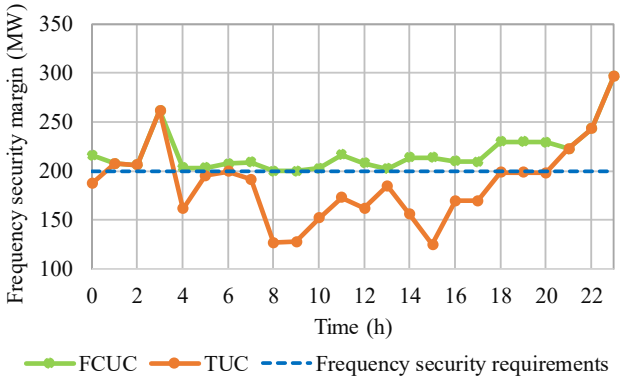

Fig. 9. Comparison of frequency security margins of TUC and FCUC.

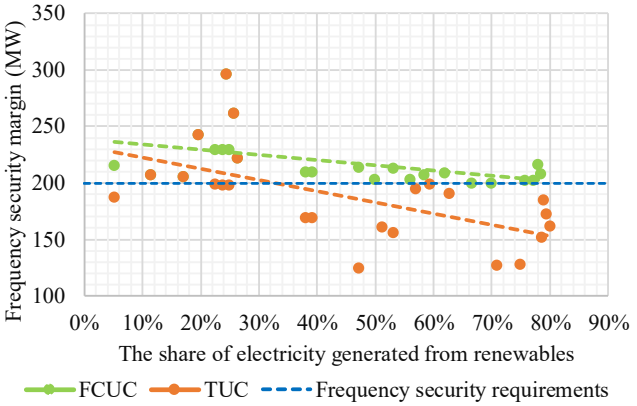

Fig. 10. The relationship between frequency security margin and share of VRE in power generation.

C. *Sensitivity Analysis*

Fig. 11 studies the impact of VRE penetration by comparing the optimization results of TUC and FCUC. When total renewables capacity increases from 2400MW to 3600MW,

both the operating costs of FCUC and TUC decrease because more electricity is supplied by low-cost VRE. However, the operating cost difference between FCUC and TUC increases from 0.66% to 4.30%. The only difference between the two models is whether the frequency security constraints are considered or not. This reveals that frequency constraints play a more important role in the system with high penetration of VRE.

Table V illustrates the value of frequency support provided by VRE. With frequency support provided by VRE, both the operating cost and renewable curtailment can be reduced. This indicates that frequency support can lead to more cost-effective integration of VRE.

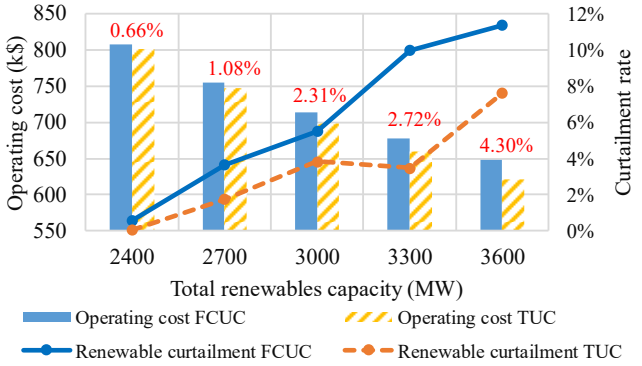

Fig. 11. Sensitivity to different shares of VRE.

TABLE V
Sensitivity to whether renewable energy provides frequency support

Case	TUC	FCUC with frequency support	FCUC without frequency support
Operating cost ($)	697864	713997	725481
Renewables curtailment	3.85%	5.51%	9.15%

Fig. 12 demonstrates the effect of the preset frequency security margin requirement ΔP on the performance of FCUC. As the requirement on the frequency security margin decreases, the operating cost and renewable curtailment can both be reduced. Operators should choose an appropriate ΔP to make a trade-off between the safety and economics of system operation. It should be noted that FCUC degrades into TUC when ΔP is lower than 120 MW. In other words, frequency constraints are ineffective when the frequency security margin requirement is low enough.

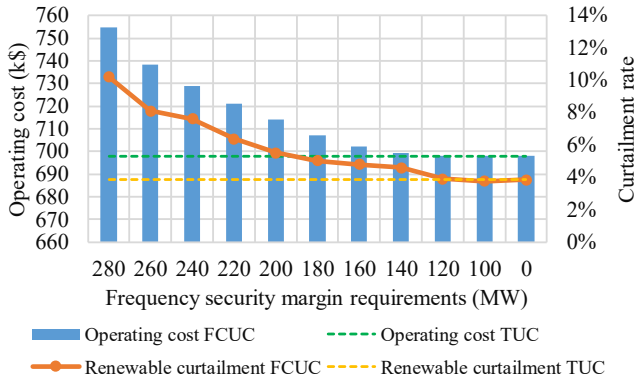

Fig. 12. Sensitivity to different frequency security margin requirements.

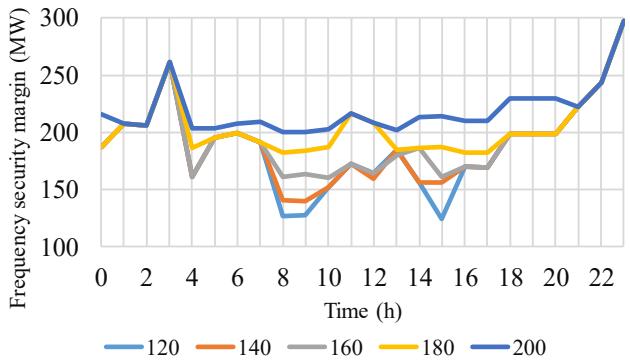

Fig. 13. System frequency security margin under different frequency security margin requirements.

Fig. 13 compares the hourly system frequency security margin under different frequency security margin requirements. As the frequency security requirement increases from 120 MW to 200 MW, the curves have significant differences between time period 7h and time period 18h just when the VRE output is high, while the curves are almost the same between hour 0 and hour 3 and between time period 21h and time period 23h when electricity is mainly generated by the conventional thermal generators. In other words, the frequency security constraints exactly take effect when the share of VRE in electricity is high.

D. Computational Performance

Compared with the TUC model, the proposed FCUC model will add $3N_T$ extra continuous variables, $(N_G+N_{PV}+N_W)\,N_T$ binary variables and $(2N_G+N_{PV}+N_W+N_J+4)\,N_T$ extra constraints. We test the TUC and FCUC under different total renewables capacities with a relative optimality gap of 0.1%. The calculation time of TUC and FCUC is shown in TABLE VI.

TABLE VI
The calculation time of TUC and FCUC under different renewables capacities

Total renewables capacity (MW)	2400	2700	3000	3300	3600
Calculation time of TUC (s)	5.449	3.795	7.540	49.906	15.359
Calculation time of FCUC (s)	5.238	92.887	1390.169	33.710	5.238

We also test the FCUC models under different frequency security margin requirements ΔP, the calculation time is listed in TABLE VII.

TABLE VII
The calculation time of FCUC under different frequency security margin requirements

ΔP	280	260	240	220
Calculation time (s)	342.053	49.945	205.505	110.564
ΔP	200	180	160	140
Calculation time (s)	1379.051	38.809	89.442	29.505

The extra complexity indeed increases the calculation time of the UC model. However, we think such additional

complexity does not hinder the merit of our paper, with three reasons: 1) The above numerical results demonstrate the effectiveness and necessity of the FCUC model. 2) The additional frequency constraints are linear. The FCUC is still a MILP model which can be well handled by current off-the-shelf solvers. 3) There are plenty of methods to accelerate the calculation of the MILP-based UC model, such as inactive constraints identification [32], tightening approach [33], parallel computing [34], etc.

VI. Case Study II: HRP-38 System

To analyze the scalability of the proposed model, we conduct a case study based on a large network, namely the HRP-38 system [35]. We make some modifications to the generation mix. The modified HRP-38 system consists of 38 nodes, 148 branches, 57 conventional thermal generators, 52 PV stations and 34 wind farms. Parameters of these generators are listed in TABLE VIII. The total installed capacity is 622.9 GW, and the annual peak load of this system is 281.1 GW.

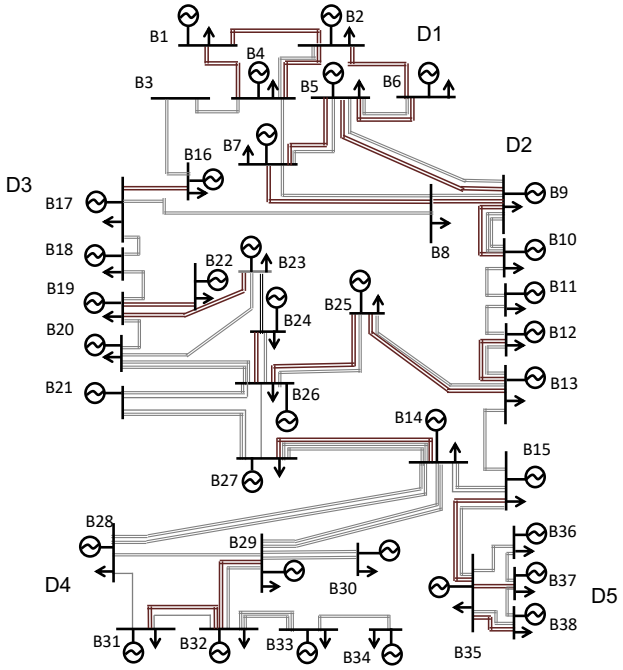

Fig. 14. Modified HRP-38 system comprised of 57 conventional units and 52 PV stations and 34 wind farms [35].

TABLE VIII
Parameters of the conventional thermal generators and VRE plants

Generation type	Coal-fired	Gas-fired	Wind	PV
Number of unit	7	50	34	52
Total Capacity (GW)	46	282.6	110.4	183.9
Inertia constant (s)	6	4	3	2
Governor constant	0.050	0.040	-	-
Droop	-	-	0.067	0.067

The forecasted load demand and VRE outputs of the selected typical day are shown in Fig. 15. The maximum power imbalance is set to 16 GW. The results of FCUC and TUC are shown in Fig. 16. The frequency security margin of TUC is below the set requirements, which may lead to frequency instability when facing such contingency. While FCUC could maintain the frequency security margin above the requirements. TABLE IX compares the operating cost and renewable curtailment of TUC and FCUC. Imposing frequency constraints leads to a slight increase in operating cost and renewables curtailment.

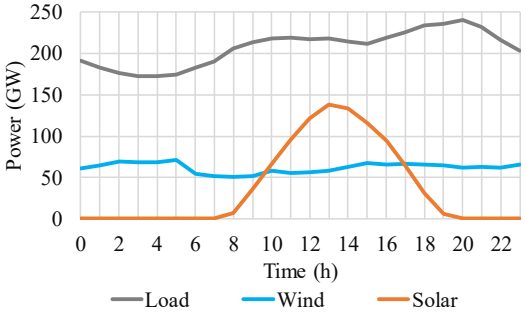

Fig. 15. Forecasted load demand and VRE outputs.

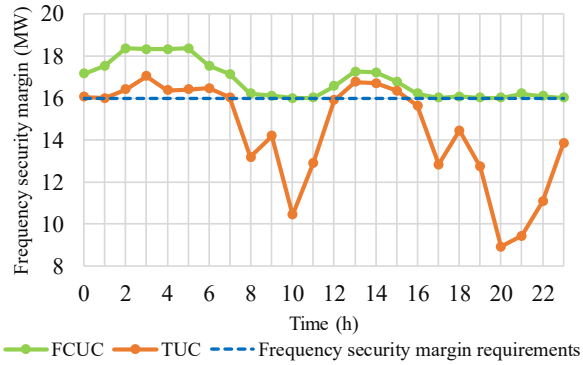

Fig. 16. Comparison of frequency security margins of TUC and FCUC.

According to the results in Fig.16, for the TUC model, synchronous units are quickly shut down or ramped down from time period 8h to 12h due to the increase of PV generation and they are quickly started or ramped up from time period 16h to 20h due to the decrease of PV generation. This leads to the inadequacy of the frequency security margin. For the FCUC model, more synchronous thermal generators are scheduled ramp-down from time period 8h to 12h in order to keep enough synchronous units online, and ramp demand is allocated among more synchronous thermal generators from time period 16h to 20h such that more generators keep adequate space for participating in frequency response.

TABLE IX
Comparison of the results of TUC and FCUC

	Operating cost (10^8 CNY)	Wind curtailment	PV curtailment
FCUC	6.98896	5.13%	8.80%
TUC	6.96953	5.06%	7.92%

VII. Conclusions

The continuous increase of VRE penetration challenges the frequency security of the power system. To address this issue, this paper proposes the concept of frequency security margin and incorporates the frequency security constraints into the UC model. Case studies on a modified IEEE RTS-79 system and HRP-38 system are carried out to verify the effectiveness of the

proposed method. The results suggest that: 1) Imposing frequency security constraints would improve the system frequency regulation ability through scheduling more thermal generators online or curtailing some VRE. Although the frequency security constraints would indeed increase the system operating cost and renewable curtailments, the system could keep the frequency security margin above the defined threshold. 2) The impacts of VRE penetrations on system operation are analyzed with the proposed frequency security margin. In the case of IEEE RTS-79 systems, when the share of VRE in electricity generation is lower than 32%, most of system operating points meet the frequency security requirements. When the share is higher than 32%, the system may face the risk of frequency insecurity. 3) the results also indicate that the frequency security will be a non-negligible factor limiting the integration of VRE in future renewable-dominated power systems. Frequency support from VRE plants can improve the economics of system operation and the integration of high penetration renewables.

APPENDIX

Derivation of constraints (30)~(32)

The governor characteristics of conventional thermal generators can be expressed as

$$\Delta P_{mi} = -\frac{K_{mi}}{R_i}\frac{1+F_{Hi}T_{Ri}s}{1+sT_{Ri}}\Delta f \tag{37}$$

When VRE provides frequency support, the typical control method is droop control, which can be expressed as

$$\Delta P_{aj} = -\frac{1}{R_{Vj}}\frac{1}{1+sT_{Vj}}\Delta f \tag{38}$$

The form of (38) is similar to that of (37). Accordingly, droop control provided by VRE can be regarded as a special governor with $F_H = 0$ and $K_m = 1$.

The relationships between the parameters of the aggregated governor and those of multiple governors are also given in [29], as follow,

$$\begin{cases} \kappa_k = \dfrac{K_{mk}}{R_k} \\ \dfrac{1}{R} = \displaystyle\sum_{k=1}^{N}\kappa_k \\ \lambda_k = \kappa_k \Big/ \displaystyle\sum_{k=1}^{N}\kappa_k \\ F_H = \displaystyle\sum_{k=1}^{N}\lambda_k F_{Hk} \\ T = \displaystyle\sum_{k=1}^{N}\lambda_k T_{Rk} \end{cases} \tag{39}$$

We assume that the reheat time constants of thermal generators and the inverter time constants of VRE plants are the same, i.e. $T_{Ri} = T_{Vj} = T$, which is a conservative assumption.

All online thermal generators provide system inertia, while only VRE operating in the degrading mode could provide synthetic inertia.

$$H_t = \frac{\sum_i H_i S_{Bi}}{S_{Bsys}} = \frac{1}{\sum_n D_{n,t}^{Fore}}\left(\begin{array}{l}\sum_g x_{g,t}^G H_g^G P_g^{G,Max} + \sum_w u_{w,t}^W H_w^W P_{w,t}^{W,Fore} \\ +\sum_{pv} u_{pv,t}^{PV} H_{pv}^{PV} P_{pv,t}^{PV,Fore}\end{array}\right), \forall t \tag{40}$$

In order to keep load damping factor D constant at each hour, we choose the hourly load demand $\sum_n D_{n,t}^{Fore}$ as the base value of power. As for frequency support provided by VRE, we assume the synthetic inertia and droop control is proportional to their hourly forecasted output. Thus, (37) and (38) should be rewritten as

$$\Delta P_{mi} = \frac{P_i^{Max,G}}{\sum_n D_{n,t}^{Fore}}\frac{K_{mi}}{R_i}\frac{1+F_{Hi}T_{Ri}s}{1+sT_{Ri}}\Delta f \tag{41}$$

$$\Delta P_{aj} = -\frac{1}{R_{Vj}}\frac{P_j^{Fore}}{\sum_n D_{n,t}^{Fore}}\frac{1}{1+sT_{Vj}}\Delta f \tag{42}$$

According to (39), the aggregated droop coefficient $\frac{1}{R_t}$ and turbine factor F_t can be calculated as follows

$$\frac{1}{R_t} = \sum_k \frac{K_{mk}}{R_k} = \frac{1}{\sum_n D_{n,t}^{Fore}}\left(\begin{array}{l}\sum_g u_{g,t}^G \frac{K_{mg}}{R_g^G} P_g^{G,Max} + \sum_w u_{w,t}^W \frac{1}{R_w^W} P_{w,t}^{W,Fore} \\ +\sum_{pv} u_{pv,t}^{PV} \frac{1}{R_{pv}^{PV}} P_{pv,t}^{PV,Fore}\end{array}\right), \forall t \tag{43}$$

$$\begin{aligned} F_t &= \frac{F_{Ht}}{R_t} = \frac{1}{R_t}\sum_k \lambda_k F_{Hk} = \frac{1}{R_t}\sum_k \frac{\kappa_k F_{Hk}}{\sum_k \kappa_k} = \frac{1}{R_t}\frac{1}{\sum_k \kappa_k}\sum_k \kappa_k F_{Hk} \\ &= \sum_k \frac{K_{mk}}{R_k} F_{Hk} = \frac{1}{\sum_n D_{n,t}^{Fore}}\left(\sum_g u_{g,t}^G \frac{K_{mg} F_g^G}{R_g^G} P_g^{G,Max}\right), \forall t \end{aligned} \tag{44}$$

Since droop control provided by VRE plants can be regarded as a special governor with $F_H = 0$ and $K_m = 1$, VRE plants have no impact on F_t

REFERENCES

[1] A. Ulbig, T. S. Borsche and G. Andersson, "Impact of Low Rotational Inertia on Power System Stability and Operation," *IFAC Proceedings Volumes*, vol. 47, pp. 7290-7297, 2014-01-01 2014.

[2] L. Xie, P. M. S. Carvalho, L. A. F. M. Ferreira, J. Liu, B. H. Krogh, N. Popli, and M. D. Ilić, "Wind Integration in Power Systems: Operational Challenges and Possible Solutions," *Proceedings of the IEEE*, vol. 99, pp. 214-232.

[3] N. Nguyen and J. Mitra, "An Analysis of the Effects and Dependency of Wind Power Penetration on System Frequency Regulation," *IEEE Trans. Sustainable Energy*, vol. 7, pp. 354-363, 2016.

[4] Q. Hou, E. Du, N. Zhang and C. Kang, "Impact of High Renewable Penetration on the Power System Operation Mode: A Data-Driven Approach," in *IEEE Transactions on Power Systems*, vol. 35, no. 1, pp. 731-741, Jan. 2020.

[5] E. Du, N. Zhang, C. Kang, B. Kroposki, H. Huang, M. Miao and Q. Xia, "Managing Wind Power Uncertainty Through Strategic Reserve Purchasing," in *IEEE Transactions on Power Systems*, vol. 32, no. 4, pp. 2547-2559, July 2017

[6] Y. Wang, V. Silva and M. Lopez-Botet-Zulueta, "Impact of high penetration of variable renewable generation on frequency dynamics in the continental Europe interconnected system," in *IET Renewable Power Generation*, vol. 10, no. 1, pp. 10-16, 1 2016.

[7] E. Du, N. Zhang, C. Kang and Q. Xia, "A High-Efficiency Network-Constrained Clustered Unit Commitment Model for Power System Planning Studies," *IEEE Trans. Power Syst.,* vol. 34, no. 4, pp. 2498-2508, July 2019.

[8] J. F. Restrepo and F. D. Galiana, "Unit Commitment with Primary Frequency Regulation Constraints," *IEEE Trans. Power Syst.,* vol. 20, pp. 1836-1842, 2005.
[9] G. W. Chang, C. Chuang, T. Lu, and C. Wu, "Frequency-regulating reserve constrained unit commitment for an isolated power system," *IEEE Trans. Power Syst.,* vol. 28, pp. 578-586, 2013.
[10] H. Chavez, R. Baldick, S. Sharma, "Governor Rate-Constrained OPF for Primary Frequency Control Adequacy". *IEEE Trans. Power Syst.,* vol.29, no.3, pp:1473-1480, 2014.
[11] Y. Wen, W. Li, G. Huang and X. Liu, "Frequency Dynamics Constrained Unit Commitment With Battery Energy Storage," in *IEEE Transactions on Power Systems*, vol. 31, no. 6, pp. 5115-5125, Nov. 2016.
[12] H. Ahmadi and H. Ghasemi, "Security-Constrained Unit Commitment with Linearized System Frequency Limit Constraints," *IEEE Trans. Power Syst.,* vol. 29, pp. 1536-1545, 2014.
[13] P. M. Anderson and M. Mirheydar, "A low-order system frequency response model," *IEEE Trans. Power Syst.,* vol. 5, pp. 720-729, 1990-01-01 1990.
[14] F. Teng, V. Trovato and G. Strbac, "Stochastic Scheduling with Inertia-Dependent Fast Frequency Response Requirements," *IEEE Trans. Power Syst.,* vol. 31, pp. 1557-1566, 2016.
[15] M. Paturet, U. Markovic, S. Delikaraoglou, E. Vrettos, P. Aristidou and G. Hug, "Stochastic Unit Commitment in Low-Inertia Grids," in *IEEE Trans. Power Syst.,* in press. doi: 10.1109/TPWRS.2020.2987076.
[16] L. E. Sokoler, P. Vinter, R. Baerentsen, K. Edlund, and J. B. Jorgensen, "Contingency-Constrained Unit Commitment in Meshed Isolated Power Systems," *IEEE Trans. Power Syst.,* vol. 31, pp. 3516-3526, 2016.
[17] H. Xin, Y. Liu, Z. Wang, D. Gan, and T. Yang, "A New Frequency Regulation Strategy for Photovoltaic Systems Without Energy Storage," *IEEE Trans. Sustainable Energy*, vol. 4, pp. 985-993, 2013.
[18] D. Yang, J. Kim, Y. C. Kang, E. Muljadi, N. Zhang, J. Hong, S. Song, and T. Zheng, "Temporary Frequency Support of a DFIG for High Wind Power Penetration," *IEEE Trans. Power Syst.,* vol. 33, pp. 3428-3437, 2018.
[19] M. Ebrahimi, S. A. Khajehoddin and M. Karimi-Ghartemani, "An Improved Damping Method for Virtual Synchronous Machines," in *IEEE Trans. Sustainable Energy*, vol. 10, no. 3, pp. 1491-1500, July 2019.
[20] W. Du, Q. Fu and H. F. Wang, "Power System Small-Signal Angular Stability Affected by Virtual Synchronous Generators," *IEEE Trans. Power Syst.,* vol. 34, no. 4, pp. 3209-3219, July 2019.
[21] U. Markovic, Z. Chu, P. Aristidou and G. Hug, "LQR-Based Adaptive Virtual Synchronous Machine for Power Systems With High Inverter Penetration," in *IEEE Trans. Sustainable Energy*, vol. 10, no. 3, pp. 1501-1512, July 2019.
[22] Y. Yoo, S. Jung and G. Jang, "Dynamic Inertia Response Support by Energy Storage System with Renewable Energy Integration Substation," in *Journal of Modern Power Systems and Clean Energy*, vol. 8, no. 2, pp. 260-266, March 2020.
[23] J. Liu, D. Yang, W. Yao, R. Fang, H. Zhao, and B. Wang, "PV-based virtual synchronous generator with variable inertia to enhance power system transient stability utilizing the energy storage system," *Protection Control Modern Power Syst*., vol. 2, no. 2, pp. 429–437, Dec. 2017.
[24] V. Gevorgian, Y. Zhang and E. Ela, "Investigating the Impacts of Wind Generation Participation in Interconnection Frequency Response," *IEEE Transactions on Sustainable Energy*, vol. 6, pp. 1004-1012, 2015.
[25] F. Teng and G. Strbac, "Assessment of the Role and Value of Frequency Response Support from Wind Plants," *IEEE Trans. Sustainable Energy*, vol. 7, pp. 586-595, 2016.
[26] Z. Chu, U. Markovic, G. Hug and F. Teng, "Towards Optimal System Scheduling with Synthetic Inertia Provision from Wind Turbines," in *IEEE Transactions on Power Systems*, in press, doi: 10.1109/TPWRS.2020.2985843.
[27] P. Kundur, Power system stability and control, New York, NY, USA:McGraw-Hill, 1994.
[28] T. Shintai, Y. Miura and T. Ise, "Oscillation Damping of a Distributed Generator Using a Virtual Synchronous Generator," *IEEE Trans. Power Delivery*, vol. 29, pp. 668-676, 2014.
[29] Q. Shi, F. Li and H. Cui, "Analytical Method to Aggregate Multi-Machine SFR Model with Applications in Power System Dynamic Studies," *IEEE Trans. Power Syst.*, vol. 33, pp. 6355-6367, 2018.
[30] Probability Methods Subcommittee, "IEEE Reliability Test System," *IEEE Trans. Power Apparatus and Systems*, vol. PAS-98, pp. 2047-2054, 1979.
[31] I. D. Margaris, S. A. Papathanassiou, N. D. Hatziargyriou, A. D. Hansen and P. Sorensen, "Frequency Control in Autonomous Power Systems With High Wind Power Penetration," in *IEEE Transactions on Sustainable Energy*, vol. 3, no. 2, pp. 189-199, April 2012.
[32] Q. Zhai, X. Guan, J. Cheng and H. Wu, "Fast Identification of Inactive Security Constraints in SCUC Problems," in *IEEE Transactions on Power Systems*, vol. 25, no. 4, pp. 1946-1954, Nov. 2010.
[33] B. Yan, P. B. Luh, T. Zheng, D. A. Schiro, M. A. Bragin, F. Zhao, J. Zhao and I. Lelic, "A Systematic Formulation Tightening Approach for Unit Commitment Problems," in *IEEE Transactions on Power Systems*, vol. 35, no. 1, pp. 782-794, Jan. 2020.
[34] A. Papavasiliou, S. S. Oren and B. Rountree, "Applying High Performance Computing to Transmission-Constrained Stochastic Unit Commitment for Renewable Energy Integration," in *IEEE Transactions on Power Systems*, vol. 30, no. 3, pp. 1109-1120, May 2015.
[35] Z. Zhuo, N. Zhang, J. Yang, C. Kang, C. Smith, M. J. O'Malley, and B. Kroposki, "Transmission Expansion Planning Test System for AC/DC Hybrid Grid With High Variable Renewable Energy Penetration," in *IEEE Transactions on Power Systems*. in press. doi: 10.1109/TPWRS.2019.2959508

Ziyang Zhang (S'19) received the B.S. degree in electrical engineering in 2019 from Tsinghua University, Beijing, China, where he is currently working toward the Ph.D. degree.

His research interests include renewable energy, power system operation, and power system planning.

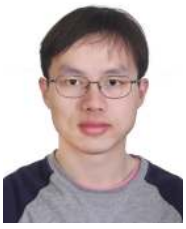

Ershun Du (M'18) received both a B.S and Ph.D. from the Electrical Engineering Department of Tsinghua University in 2013 and 2018, respectively.

His research interests include renewable energy uncertainty analysis, power system economics and planning, concentrating solar power.

Fei Teng (M'15) received the BEng in Electrical Engineering from Beihang University, China, in 2009, and Ph.D. degree in Electrical Engineering from Imperial College London, U.K., in 2015. Currently, he is a Lecturer in the Department of Electrical and Electronic Engineering, Imperial College London, U.K.

His research focuses on scheduling and market design for low-inertia power system, cyber-resilient energy system operation and control, and objective-based data analytics for future energy systems.

Ning Zhang (S'10, M'12, SM'18) received both B.S. and Ph.D. from the Electrical Engineering Department of Tsinghua University in China in 2007 and 2012, respectively.

He is now an Associate Professor at the same university. His research interests include multiple energy systems integration, renewable energy, and power system planning and operation

Chongqing Kang (M'01, SM'07, F'17) received his Ph.D. from the Electrical Engineering Department of Tsinghua University in 1997.

He is now a Professor at the same university. His research interests include power system planning, power system operation, renewable energy, low carbon electricity technology and load forecasting.